Juvenile source nature of the North Tianshan turbidites and its tectonic implication

Meng Wang[1,2] 🄳, Ming Cao[1], Da Xu[1], Youxin Chen[1], Jinjiang Zhang[3], Bo Zhang[3], Xianzhi Pei[1], Zuochen Li[1], Hai Zhou[1] and Zhian Bao[2]

[1]Key Laboratory of Western Mineral Resources and Geological Engineering, MOE, School of Earth Science and Resources, Chang'an University, Xi'an, China; [2]State Key Laboratory of Continental Dynamics, Department of Geology, Northwest University, Xi'an, China and [3]Key Laboratory of Orogenic belts and Crustal Evolution, MOE, School of Earth and Space Sciences, Peking University, Beijing, China

Abstract

Sediments within accretionary complexes, preserving key information on crust growth history of Central Asian Orogenic Belt, did not get enough attention previously. Here, we conduct comprehensive geochemical study on the turbidites from the North Tianshan Accretionary Complex (NTAC) in the Chinese West Tianshan orogen, which is a good example of sediments derived from juvenile materials. The turbidites, composed of sandstone, siltstone, and argillaceous siliceous rocks, are mainly Carboniferous. All the investigated samples have relatively low Chemical Index of Alteration values (35–63) and Plagioclase Index of Alteration values (34–68), indicating relatively weak weathering before erosion and deposition. The sandstone and siltstone, and slate samples display high Index of Compositional Variability values of 0.89–1.50 and 0.89–0.93, suggesting a relatively immature source. The sandstones and siltstones were mainly derived from intermediate igneous rocks, and the slates from felsic igneous rocks, formed in oceanic/continental arc settings. The investigated samples roughly display high positive $\varepsilon Nd(t)$ values (mainly at +5.5 to +7.9, except one spot at +0.8), with corresponding Nd model ages at 672 Ma–522 Ma (except one at ~1.1 Ga). Combined with the previous studies, we suggest that the turbidites in the NTAC were mainly derived from intermediate to felsic igneous rocks with juvenile arc signature, and thus the northern Chinese West Tianshan is a typical site with significant Phanerozoic crust growth.

1. Introduction

The Central Asian Orogenic Belt (CAOB), surrounded by the Siberia, Baltica, Tarim, and North China cratons, is a collage of microcontinents, oceanic-island arcs, seamounts, oceanic plateaus and accretionary complexes over ca. 800 million years (Sengör *et al.* 1993; Jahn *et al.* 2004; Kröner *et al.* 2014). It has been widely accepted that the CAOB, with the largest area of crustal growth in the Phanerozoic, is one of the largest accretionary orogens on Earth (Sengör *et al.* 1993; Jahn *et al.* 2000, 2004; Windley *et al.* 2007; Xiao *et al.* 2013; Safonova, 2017). The identification of many intro-oceanic arcs, accretionary complexes, oceanic plate strata, and MORB-OIB derived blueschist belts within the CAOB, and positive Nd-Hf isotope character of magmatic rocks are key evidence for its juvenile character (Jahn *et al.* 2000, 2004; Safonova, 2017). However, some researchers stated that the volume of truly juvenile crustal material in the CAOB has been overestimated (Kröner *et al.* 2014, 2017). One reason is that there are many microcontinents with Precambrian basement in the CAOB (Kröner *et al.* 2014; Long & Huang, 2017). Even in juvenile crustal regions such as the Chinese Altai, ancient crustal materials were identified (Xu *et al.* 2015; Zhang *et al.* 2017), and the Hf-in-zircon isotope data reveal recycled crust (Kröner *et al.* 2017). Another reason might be whether the intra-oceanic arcs were correctly recognized (Kröner *et al.* 2017). Therefore, the proportion of juvenile and recycled crust for crust growth during the late-stage evolution of the CAOB is still an open question.

Pacific-type convergent margins are major sits of continental growth and crustal recycling. The proportions of juvenile and recycled crust are generally estimated by the amount and geochemical signature of granitoids in the supra-subduction zone. However, the under-estimation of crust growth caused by erosion of magmatic rocks during geological processes is generally ignored. These eroded materials were transported and deposited in the trench and adjacent for-arc and back-arc basins, forming characteristic clastic sedimentary rocks in accretionary complexes (Safonova *et al.* 2022a) These clastic rocks are compositionally similar to their source rocks and contain detrital zircons, recording crystallization ages and source characters information of their parental igneous rocks. If sediments were derived mainly from eroded intra-arc crust, then they can be regarded as contribution of continental growth. Therefore, the study of sediment recycling might be important in evaluating the proportion of continental growth. Despite a few recent studies (Safonova *et al.* 2022a, b), accretionary
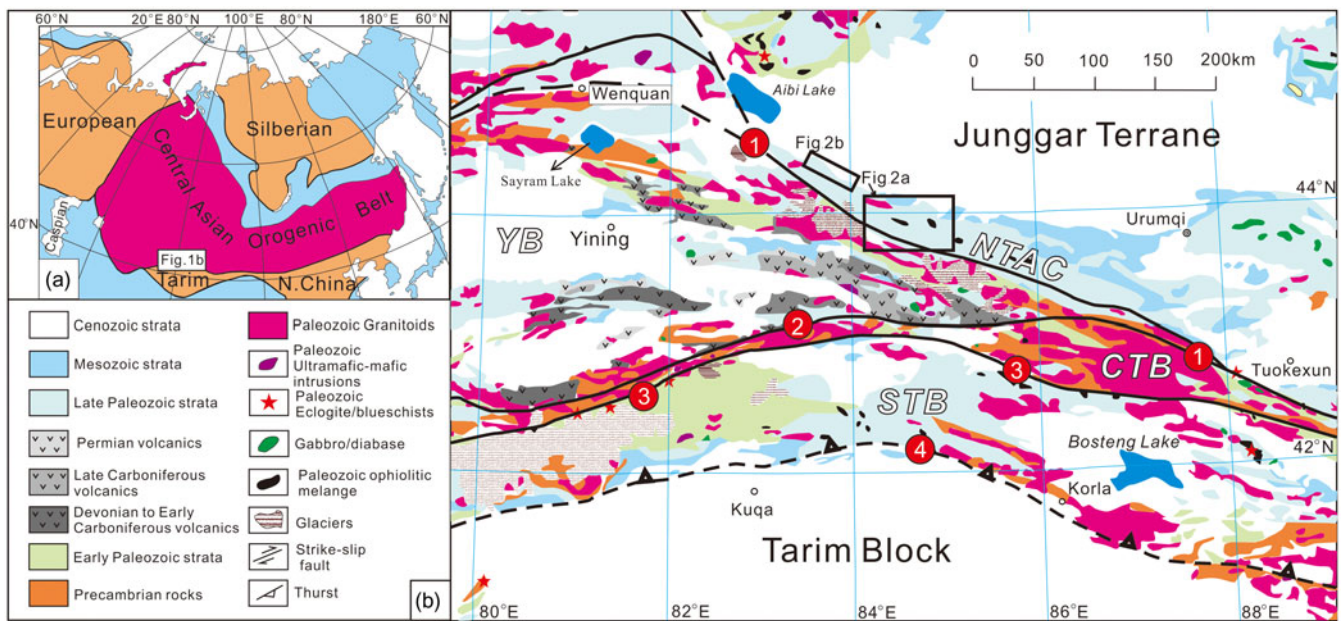
Figure 1. (Colour online) (a) Tectonic framework of the Central Asian Orogenic Belt (modified after Şengör *et al.* 1993 and Xiao *et al.* 2013). (b) Geological map of the Chinese West Tianshan Orogen and adjacent regions (modified after Gao *et al.* 2009). Numbers in circle refer to the tectonic boundaries: 1) North Tianshan Suture Zone; 2) Nikolaev line-North Nalati Suture Zone; 3) Southern Central Tianshan Suture Zone; and 4) North Tarim Thrust. Abbreviations for the tectonic unites are: NTAC = North Tianshan Accretionary Complex; YB = Yili Block; CTB = Central Tianshan Block; STB = South Tianshan Belt.

complexes, as major component of the CAOB, lack detailed study especially on assessing CAOB late-stage crustal growth.

The Chinese West Tianshan Orogen is located in the southwest part of the CAOB (Fig. 1a). The northern part of the Chinese West Tianshan Orogen is composed of late Paleozoic accretionary complex, including flysch type volcano-sedimentary rocks and some ophiolite fragments, in response to evolution of the North Tianshan Ocean. Previous studies mainly focus on the petrology, geochronology and geochemistry of the ophiolites (Xiao *et al.* 1992; Xu *et al.* 2006a, b; Li *et al.* 2015; Feng & Zhu, 2018; Zheng *et al.* 2019), but studies on the sedimentary rocks are weak. Recently, our group reported detrital zircon U-Pb geochronology and Lu-Hf isotope characteristics of the turbidites, suggesting significant Carboniferous magmatism and continental growth (Wang *et al.* 2018a). In this paper, we present whole rock geochemistry and Sr-Nd isotope for the turbidites in the North Tianshan Accretionary Complex (NTAC) (Fig. 2) to further constrain their provenance and tectonic setting of their parental igneous rocks and evaluate their contribution for continental growth.

2. Geological background

The CAOB, also known as the modified Altaids, occupies an immense area in central Asia (Fig. 1a). The Tianshan orogenic belt, presently extending for more than 2500 km from west to east through Uzbekistan, via Tajikistan, Uzbekistan, and Kyrgyzstan to northwestern China, is an important constituent part of the CAOB. The Chinese Tianshan can be subdivided into the Western Tianshan and East Tianshan, which are different both in topography and evolutionary history, roughly along the longitude ~90°E (Xiao *et al.* 2013). The Chinese West Tianshan Orogen can be further subdivided into the North Tianshan Accretionary Complex (NTAC), the Yili Block (YB), the Central Tianshan Block,

and the South Tianshan Belt, which are separated by the North Tianshan, North Narat, and South Tianshan faults (Fig. 1b).

The YB is a triangular shaped micro-continent which mainly Neoproterozoic basement rocks and extends over 1000 km across NW China, Kazakhstan, and Kyrgyzstan (Wang *et al.* 2006). The center of the YB is covered by Cenozoic sediments. The basement rocks are exposed in the northern and southern side of the YB. Ordovican to Silurian intrusive rocks which might be related to the early stage subduction of the NTSO, are found in the Wenquan area of the northwestern YB (Wang *et al.* 2012; Huang *et al.* 2013). Late Paleozoic volcano-sedimentary rocks and intrusive rocks are widely distributed in both sides of the block and were suggested to be related to the subduction of the North Tianshan and South Tianshan oceans (Wang *et al.* 2022 and references therein).

The Central Tianshan Block is a strip-like arc terrane with Precambrian basement (Gao *et al.* 2009). It approximately corresponds to the Narat Range in the west and extend from the Baluntai area to Xingxingxia area in the east. The basement rocks are mainly Meso- to Neo-proterozoic schists, paragneiss, and granitic gneisses (Hu *et al.* 2010; Wang *et al.* 2014; Gao *et al.* 2015; Huang *et al.* 2017). Paleozoic volcanic and intrusive rocks are widely exposed and were formed due to subduction and closure of the Terskey and South Tianshan oceans (Xu *et al.* 2013; Wang *et al.* 2016a, 2022; Zhong *et al.* 2017).

The South Tianshan Belt is a wide tectonic unit bounded by the southern Central Tianshan Fault and the northern Tairm Fault (Xiao *et al.* 2013). It was formed as a result of the consumption of the South Tianshan ocean and subsequent collision between the Tarim Craton and Yili-Central Tianshan Block (Charvet *et al.* 2011; Xiao *et al.* 2013; Wang *et al.* 2018b; Huang *et al.* 2020). The South Tianshan Belt is composed of Cambrian to Carboniferous limestone, siliciclastic turbidites, cherts, and interlayered volcanics (Jiang *et al.* 2014). Permian unconformably overlie the former strata (Wang *et al.* 2014). Several ophiolite fragments with ages

ranging from 590 to 320 Ma have been identified within the South Tianshan Belt (Jiang *et al.* 2014; Wang *et al.* 2011, 2018b and references therein). Ophiolites that experienced high pressure metamorphism were also reported in the Akeyazi, NW China (Gao *et al.* 1995), and Atbashi, Kyrgyzstan (Hegner *et al.* 2010).

The NTAC located between the Junggar terrane and the YB, extends over 300 km along the northern margin of the North Tianshan. It consists mainly of two of two different lithologies: 1) the ophiolitic remnants (Wang *et al.* 2006; Xu *et al.* 2006a; Han *et al.* 2010) and 2) the Carboniferous volcano-sedimentary rocks which were regarded as turbidites (Wang *et al.* 2006). The ophiolites exposed discontinuously over an area of ~250 km in length and 5–15 km in width (Fig. 1(b)), and the Bayingou ophiolite is one of the best outcrops (Xu *et al.* 2006a). Famennian-Visean conodonts and radiolarians had been found from the cherts within the NTAC (Xiao *et al.* 1992). Gabbro and plagiogranite from the Bayingou ophiolite have SHRIMP U-Pb age of 344 Ma and 325 Ma (Xu *et al.* 2006a, b). Plagiogranite from the Kuitun River section were dated at 343 Ma (Li *et al.* 2015). Layered and massive gabbros in the Jinghe ophiolite were dated to be 381 and 382 Ma (Zheng *et al.* 2019). There exist several different perspectives about the nature of the North Tianshan ophiolites, i.e. 1) remnant of a 'Red Sea type' oceanic basin (Xia *et al.* 2004; Xu *et al.* 2006a, b), 2) remnants of a long-lived wide ocean (Yang *et al.* 2018), 3) products related to ridge subduction (Li *et al.* 2015), and 4) ophiolite formed in forearc setting (Feng & Zhu, 2018).

The turbiditic sequence in the NTAC consist mainly of tuffaceous sandstone, siltstone, tuff, and black argillite alternations (Fig. 3). The tuffaceous sandstone ranges in thickness from a few centimeters to 50 centimeters, but mostly around 10–40 cm (Fig. 3a, b). Some deep-water ichnofossils, like *Chondrites sp.*, *Cosmorphaphe sp.*, *Helminthopsis sp. et al.*, and deep-water microfossils were found in the turbidites (Jin *et al.* 1989), indicating in a bathyal to deep-sea environment (Wang *et al.* 2006). The turbiditic sequence near the North Tianshan Fault underwent low-grade metamorphism and display a subvertical slaty cleavage (Figs. 2 and 3c), and some siltstones had turned out to be andalusite schists (Wang *et al.* 2006). Age of the turbidites were constrained to be Devonian to Carboniferous based on fossils discovered in the chert and limestone (XBGMR, 1993). However, our recent study shows that the turbidites have the youngest DZ ages of 312–303 Ma, constraining the maximum depositional time of the turbidites to the late Carboniferous (Wang *et al.* 2018a; Bai *et al.* 2020).

Volcanic rocks, represented by the Arbasay Formation, also exist within the NTAC. The Arbasay Formation, which is mainly composed of volcanic rocks in the lower part and volcaniclastic rocks in the upper part, exposes to the north of the Bayingou ophiolite (Wang *et al.* 2016a). The Arbasay Formation was previously regarded as early Permian in age, because it unconformably overlies the upper Carboniferous Qianxia Formation and is covered by the upper Permian Quanzijie Formation (XBGMR, 1993). However, zircons from the volcanic rocks and tuff of the Arbasay Formation were dated at 315–305 Ma, indicating a Late Carboniferous age (Liu *et al.* 2015; Wang *et al.* 2017; Bai *et al.* 2020). The volcanic rocks from the Arbasay Formation include basalt, andesite, dacite, and rhyolite, dominated by andesites (Liu *et al.* 2015; Bai *et al.* 2020). The volcanic rocks display arc-like geochemical signatures, indicating that they are subduction related and might have formed during the tectonic transition from compression to extension (Wang *et al.*, 2017; Bai *et al.* 2020).

3. Sampling and analytical methods

Fifteen clastic rock samples, mainly fine-grained sandstones and siltstones, and 4 slate samples were collected from the NTAC for geochemical studies. We also selected 6 sandstones to determine their Rb-Sr and Sm-Nd isotope compositions. The detailed sampling locations are illustrated in Fig. 2. Representative petrographic characteristics of the studied samples are shown in Fig. 3c-d.

Whole-rock major and trace element analyses were conducted at the SKLCD, Norwest University, China. The rock samples were first crushed into small fragment and cleaned in distilled water, dried, and then ground into powder. Major elements were determined by XRF method, while trace and rare earth elements were analyzed using an ICP-MS (PE 6100 DRC). Analytical precision and accuracy are better than 5% for major elements, 2% for most trace elements and 10% for transition metals. Detailed procedures and working conditions are described in Dong *et al.* (2011).

The Rb-Sr and Sm-Nd isotopes of the samples were analyzed at the Wuhan SampleSolution Analytical Technology Co., Ltd., Wuhan, China. All chemical preparations were performed on class 100 work benches within a class 1000 over-pressured clean laboratory. Whole rock Sr-Nd isotope analyses were performed on a Neptune Plus MC-ICP-MS (Thermo Fisher Scientific, Dreieich, Germany). Analyses of the NIST SRM 987 standard solution yielded $^{87}Sr/^{86}Sr$ ratio of 0.710243 ± 4 (2 SD, n = 7), which is the same with published value of 0.710241±12 within error (Zhang *et al.* 2020). The USGS reference materials BCR-2 (basalt) and RGM-2 (rhyolite) yielded $^{87}Sr/^{86}Sr$ ratios of 0.704990 ± 6 and 0.703960 ± 6, respectively, consistent with the published values (Zhang *et al.* 2020; Li *et al.* 2012). Analyses of the GSB 04-3258-2015 standard yielded $^{143}Nd/^{144}Nd$ ratio of 0.512441 ±2 (2SD, n = 7), which is identical within error to the published values (0.512439 ± 10 (2SD), Li *et al.* 2017). In addition, the USGS reference materials BCR-2 (basalt) and RGM-2 (rhyolite) yielded $^{143}Nd/^{144}Nd$ ratios of 0.512644 ± 7 and 0.512802 ± 6, respectively, which are within error to their published values (Zhang *et al.* 2020).

4. Analytical results

4.a. Major element

Analytical results of whole-rock major and trace elements are listed in Table 1. The sandstone/siltstones display a wide range of SiO_2 contents varying from 49.73 wt %–71.25 wt %, but mostly lower than 65 wt % (average 60.28 wt %), which are below or slightly higher than that of average upper continental crust (UCC; 66.6 wt %) (Taylor *et al.* 1981) and post-Archaean Australian shales (PAAS; 62.4 wt %) (Taylor and McLennan, 1985). They also have variable Na_2O (2.30–5.58 wt %) and K_2O (0.52–4.85), with Na_2O/K_2O ratios between 0.6 and 9.2. The samples have high $Fe_2O_3^T$ (av. 5.31 wt %), Al_2O_3 (av. 16.05 wt %) and MgO (av. 2.15 wt %) contents, suggesting a more mafic to intermediate source. The slates show higher SiO_2 contents of 66.78 wt %–73.21 wt %, higher than those in UCC and PAAS. They also have lower $Fe_2O_3^T$ (av. 3.57 wt %), MgO (1.44 wt %), and Al_2O_3 (av. 13.56 wt %) than the sandstones, suggesting more quartz and less mafic minerals in the source of the slates. Although the sandstones and the slates have different major element compositions, they all plot in the greywacke field in the rock type discrimination diagram (Fig. 4). The Na_2O/Al_2O_3 ratios of 0.17–0.36 for the studied samples are also typical of
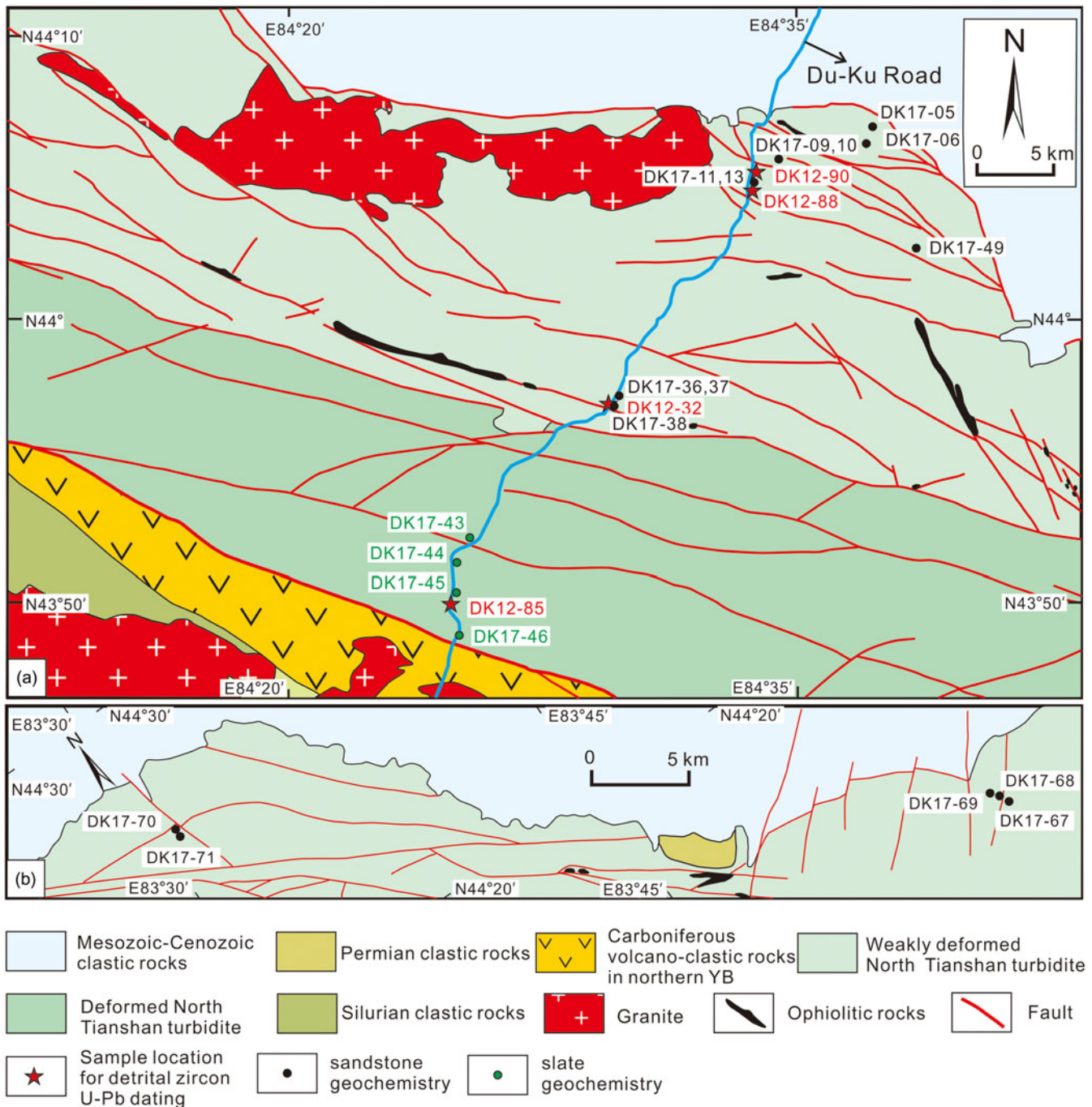
Figure 2. (Colour online) Geological map of the study area (modified from XBGMR, 1993), showing sample locations. The sample locations for detrital zircon U-Pb dating are from Wang *et al.* (2018a).

greywackes. Negative correlations can be observed for all the samples between SiO_2 and TiO_2, Al_2O_3, Fe_2O_3, and MgO (Figures not shown), indicating weak major element fractionation during sedimentation, i.e., they are first cycle sediments (Safonova *et al.* 2022a).

4.b. Trace and rare earth element

Most of the studied samples have lower rare earth and other incompatible element concentrations than PAAS (Fig. 5). Most of the sandstone/siltstone samples have low rare earth element (REE)

contents of from 60 ppm to 99 ppm, except for one sample TS17-70 which has total REE values of 133 ppm. The slates have relatively higher ΣREE values of 110 ppm–121 ppm, with one exception (TS17-44) of 76 ppm. Both the sandstone/siltstone and slate samples display are enriched in LREE and depleted in HREE (Fig. 5c, d), with $(La/Yb)_N$ ratios of 2.09–6.58 and 4.88–7.00, respectively (Table 1). Most sandstone/siltstone samples display weak positive Eu anomalies $((Eu/Eu^*) = 1.01–1.3)$, and two samples show weak negative Eu anomalies $((Eu/Eu^*) = 0.98$ and 0.88), similar to that of the Late Carboniferous basaltic rocks in the NTAC (Fig. 5c). In comparison, the slate samples have moderate

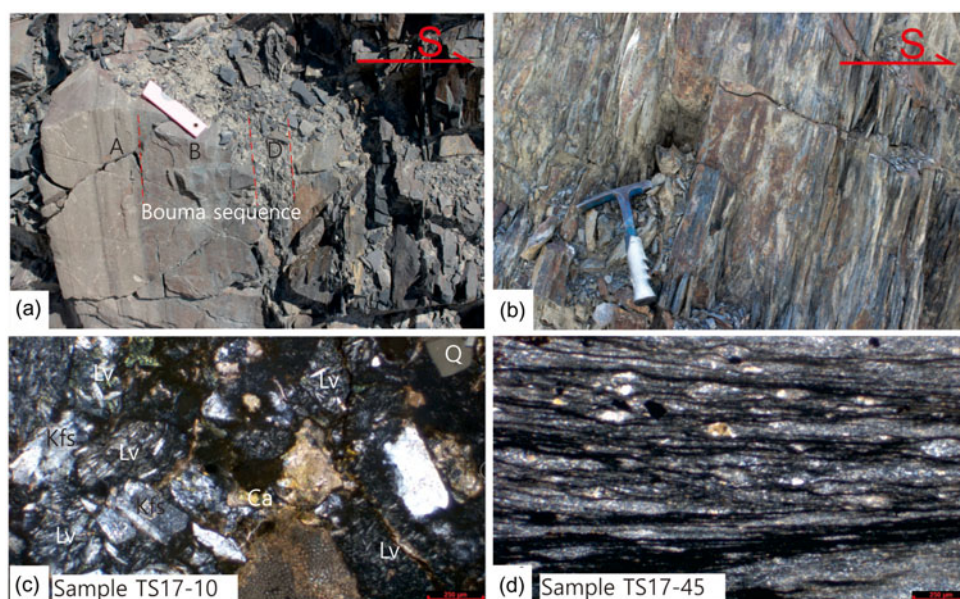**Figure 3.** (Colour online) Representative outcrop (a, b; from Wang *et al.* 2018a) and microphotographs (c, d) of the turbidites from the NTAC.

negative Eu anomalies ((Eu/Eu*) = 0.77–0.87, with one exception of 1.02), which is a feature of intermediate to felsic magmatic rocks that undergone fractional crystallization of plagioclase.

In the primitive mantle normalized multielement spectra (Fig. 5a, b), all the samples show clear Nb depletion compared to La (Nb/La$_{pm}$ = 0.2-0.8) and Th (Nb/Th$_{pm}$ = 0.1-0.2), suggesting their derivation from supra-subduction/arc volcanic rocks (Briqueu *et al.*1984; Safonova *et al.* 2022a)

4.c. Sr-Nd isotope

We conducted Rb-Sr and Sm-Nd isotope analyses for six sandstone samples from the NTAC. The samples display ^{147}Sm/^{144}Nd ratios between 0.129367 and 0.163533, and ^{143}Nd/^{144}Nd ratios between 0.512543 and 0.512975 (Table 2). Most samples have high positive $\varepsilon_{Nd}(t)$ values (+5.5 to +7.9), with only one exception($\varepsilon_{Nd}(t)$ = +0.8) (Fig. 6), and the T$_{DM2}$ values are mainly from 0.63 to 0.45 Ga (with one exception at ~1.0 Ga) (Table 2).

5. Discussion

5.a. Influence of chemical weathering and recycling

The geochemical compositions of clastic rocks are dominated controlled by, and thus can used to constrain weathering conditions and recycling of, their source rocks (Nesbitt and Young, 1984; Mclennan *et al.* 1993; Fedo *et al.* 1995). Some parameters, such as the chemical index of alteration (CIA), the plagioclase index of alteration (PIA), and index of compositional variability (ICV), are frequently used to quantify the degree of chemical weathering and composition maturity of the source rocks (Nesbitt and Young, 1984; Cox & Lowe, 1995).

The CIA values of the sandstone/siltstone samples are 35–56 (average 52) and slate samples are 56–63 (average 59). However, the CIA values could be influenced by potassium metasomatism during diagenesis, so it is necessary to use the A-CN-K triangle diagram to identify it and make corrections. In the A-CN-K diagram (Fig. 7a), the sandstone/siltstone samples define a weathering trend line that does not parrel to the A-CN line, and reflect potassium metasomatism. The point of intersection

between the weathering trend line and the Pl-Kfs line is near the plot of the tonalite (Fig. 7a). This means that the average composition of the source rocks is equal to intermediate rocks. The corrected initial CIA values of the sandstones and siltstones were slightly higher than the calculated CIA, but still lower than 60 (Fig. 7a). The slates plot near the granite field with limited weathering towards illite (Fig. 7a), reflecting a dominate felsic rock source. The corrected CIA values of the sandstone/siltstones are close to the CIA values of NASC and Archean greywacke sandstones (58; Condie, 1993), but much lower than that of PAAS (70; Taylor and McLennan, 1985). This suggests that the source rocks of the turbidites experienced low to moderate weathering before erosion and deposition. In addition, the PIA values of sandstone/siltstone (34–67, average 51) and slate samples (58–68, average 63) are both lower than that of the PAAS (Fedo *et al.* 1995), also indicating a relatively low degree of chemical weathering.

The ICV values are used to reflect the maturity of the source rocks of clastic rocks (Cox & Lowe, 1995). Sedimentary rocks which were derived from a source dominated by clay minerals generally have low ICV values, while those sourced from an immature source with high percentage of nonclay minerals commonly possess high IVC values (Van de & Leake, 1985). Both the sandstone/siltstone and slate samples display high ICV values of 0.89–1.50 and 0.89–0.93 (Fig. 7b), higher than the PAAS, suggesting a relatively immature source. In the Th/Sc–Zr/Sc plot (Fig. 7c), the samples show a trend of compositional variation instead of sedimentary recycling. The sandstone/siltstone samples have Th/U ratios lower than that of the UCC (3.8; Taylor and McLennan, 1985), while the slate samples have higher Th/U ratios than the UCC (Fig. 7d), suggesting that the sandstones/siltstones were derived from source rocks with less weathering than that of the slates.

The SiO$_2$/Al$_2$O$_3$ ratio is also an index for sedimentary maturity because quartz has stronger weathering resistance than feldspars, mafic minerals, and lithic grains (Roser *et al.* 1996; Zhang, 2004). The average values range from ~3.0 to ~5.0 for unaltered basic and felsic igneous rocks, while values >5.0–6.0 in sediments are an indication of progressive maturity (Zhang, 2004). The sandstone/

Table 1. Whole rock geochemical composition of the Carboniferous turbidites in the NTAC

Sample	TS17-05	-06	-10	-11	-13	-36	-37	-38	-49	-67	-68	-09	-69	-70	-71	-43	-44	-45	-46
Lithology	sandstone											siltstone				slate			
SiO_2	58.48	49.73	58.35	53.17	55.44	61.71	62.27	58.04	60.90	63.67	64.15	55.49	71.25	63.65	67.88	71.19	73.21	66.78	72.64
Al_2O_3	16.93	15.21	16.07	16.04	16.25	16.99	15.81	16.85	15.97	17.05	17.19	14.58	13.07	17.02	15.65	13.68	12.61	14.99	12.96
$Fe_2O_3^T$	7.03	3.81	7.13	7.45	5.60	4.16	3.59	8.03	7.03	4.44	4.40	5.43	3.34	4.68	3.59	3.03	3.97	3.84	3.45
MgO	2.95	1.29	2.50	5.14	2.87	1.72	1.24	3.32	2.26	1.33	1.57	1.68	1.17	2.06	1.13	1.63	1.42	1.18	1.54
CaO	3.54	10.93	4.44	5.81	6.65	3.59	4.97	3.96	3.72	2.72	2.18	7.60	2.34	0.72	1.73	0.98	0.32	1.95	0.84
Na_2O	4.07	4.15	4.78	3.33	3.94	4.10	3.17	3.89	4.20	4.34	3.91	4.09	2.30	3.00	5.58	2.55	2.54	3.33	2.15
K_2O	1.57	1.32	0.52	1.61	2.02	2.57	3.89	1.51	1.84	2.72	3.42	2.21	3.50	4.85	1.49	4.01	2.61	2.69	3.69
MnO	0.09	0.53	0.12	0.07	0.11	0.06	0.07	0.14	0.15	0.07	0.06	0.29	0.08	0.07	0.12	0.24	0.06	0.10	0.15
TiO_2	0.81	0.72	1.10	0.80	0.76	0.56	0.47	0.97	1.00	0.79	0.64	0.67	0.50	0.69	0.41	0.39	0.40	0.50	0.44
P_2O_5	0.17	0.20	0.19	0.17	0.16	0.16	0.12	0.18	0.22	0.18	0.18	0.24	0.11	0.20	0.09	0.11	0.08	0.10	0.09
LOI	4.23	12.01	4.66	6.27	6.06	4.20	4.23	3.00	2.61	2.53	2.14	7.56	2.14	2.84	2.19	1.99	2.69	4.43	1.92
Total	99.87	99.90	99.86	99.85	99.86	99.84	99.83	99.88	99.89	99.84	99.84	99.85	99.81	99.77	99.87	99.79	99.91	99.89	99.88
CIA	54	35	50	56	52	52	52	54	51	54	56	48	54	53	53	58	63	56	59
PIA	55	34	50	48	44	52	45	54	52	55	58	38	54	67	54	62	68	58	65
ICV	1.2	1.5	1.3	1.5	1.3	1.0	1.1	1.3	1.3	1.0	0.9	1.5	1.0	0.9	0.9	0.9	0.9	0.9	0.9
Li	32	17.0	22	47	27	19.0	21	26	17.6	17.1	19.8	19.7	17.8	28	22	29	32	26	29
Be	1.10	0.75	0.80	0.78	1.02	1.37	1.40	0.50	0.84	1.29	1.46	0.60	1.95	2.77	1.65	1.29	1.30	1.60	2.10
Sc	13.9	22	21	23	14.2	8.91	8.58	31	32	9.42	9.99	19.6	8.41	10.0	6.00	6.24	8.21	8.65	8.66
V	208	70	268	266	228	85	68	251	202	105	95	99	67	60	61	63	71	69	42
Cr	41	16.1	25	114	170	25	19.4	30	11.7	26	28	38	14.0	4.21	10.6	9.97	22	18.3	12.7
Co	14.4	8.95	16.9	25	17.5	5.62	7.53	20	13.1	10.9	9.45	11.9	7.94	3.72	4.99	6.76	7.57	4.89	4.64
Ni	21	10.5	14.7	64	45	11.0	10.4	18.6	6.59	10.8	14.4	22	9.36	2.76	6.71	34.8	14.8	8.93	15.2
Cu	42	22	44	58	51	16.5	38	57	27	25	28	38	40	31	59	26	15.8	23	34
Zn	86	83	111	82	70	63	58	110	97	75	75	79	73	77	58	53	75	68	62
Ga	20	16.6	21	19.4	18.0	17.6	16.4	19.3	21	18.8	19.0	15.8	16.7	28	13.3	15.6	15.5	19.0	16.3
Rb	16.9	17.3	7.76	19.1	24	33	88	18.4	16.7	28	38	22	91	171	21	134	53	53	114
Sr	403	305	480	535	578	420	433	366	329	491	461	411	333	258	401	245	122	210	203
Zr	114	79.5	142	71	58	85	135	129	145	151	153	162	174	295	203	153	70	218	172
Nb	2.97	2.26	2.56	2.03	2.37	4.70	4.30	2.16	2.05	4.50	4.76	4.35	5.38	11.4	9.89	8.29	5.91	7.16	6.86
Mo	0.60	0.57	0.35	0.26	0.27	0.22	0.36	0.28	0.76	0.27	0.21	1.04	0.83	0.23	0.16	0.52	0.81	0.38	0.10

(Continued)

Table 1. (*Continued*)

In	0.07	0.06	0.06	0.06	0.05	0.04	0.04	0.04	0.06	0.05	0.05	0.05	0.06	0.08	0.04	0.04	0.05	0.06	0.05
Cs	1.73	2.07	0.41	1.65	1.47	2.93	4.20	1.02	0.83	1.35	1.94	0.79	2.00	5.49	1.54	6.02	4.27	4.18	5.12
Ba	460	161	119	478	314	617	689	160	185	581	687	410	1022	1257	176	1171	193	198	467
Hf	3.74	3.31	3.68	2.31	2.40	3.51	3.38	3.25	3.77	3.62	3.75	4.11	4.28	7.15	5.07	4.14	3.05	5.60	4.49
Ta	0.29	0.29	0.41	0.21	0.21	0.47	0.52	2.46	1.44	0.30	0.34	0.47	0.41	0.68	1.00	0.76	0.64	0.71	0.62
W	0.38	0.53	0.37	0.26	0.34	0.64	0.59	0.57	0.33	0.51	0.40	0.75	0.41	1.13	0.44	0.98	0.64	0.82	0.86
Tl	0.23	0.09	0.05	0.23	0.21	0.18	0.24	0.10	0.07	0.18	0.21	0.12	0.36	0.33	0.16	0.51	0.27	0.27	0.47
Pb	9.00	4.35	5.99	7.03	6.60	8.10	9.02	3.74	4.55	10.1	10.7	10.7	17.9	9.61	19.0	17.8	9.31	13.4	9.90
Bi	0.07	0.02	0.03	0.06	0.05	0.03	0.03	0.01	0.02	0.06	0.09	0.04	0.08	0.07	0.12	0.09	0.06	0.09	0.08
Th	2.88	1.38	1.84	1.74	1.68	4.46	4.30	1.35	1.38	2.81	3.73	3.70	4.90	10.0	11.3	11.8	5.08	8.93	8.18
U	1.04	0.52	0.52	0.63	0.71	1.02	1.21	0.42	0.50	0.83	1.02	1.15	1.51	3.04	3.24	3.12	1.18	2.11	1.54
Y	21	34	18.9	14.2	15.3	16.6	16.7	17.6	29	19.0	21	23	21	25	14.6	19.4	15.3	24	24
La	11.3	10.6	8.28	8.08	9.34	17.1	15.8	8.40	9.00	15.7	17.2	13.5	17.9	23.3	12.1	22	13.9	20	20
Ce	28	23	20	25	25	23	27	21	20	28	36	31	39	51	33	53	30	41	51
Pr	3.49	3.23	2.87	2.64	2.76	4.21	3.95	2.78	3.18	4.22	4.58	4.01	4.62	6.21	3.27	5.66	3.65	5.42	5.49
Nd	15.3	15.0	13.3	11.9	12.0	16.7	15.7	12.6	15.1	17.3	18.7	17.3	18.2	25	12.6	21.0	14.0	21.5	21.3
Sm	3.67	4.01	3.34	2.79	2.87	3.37	3.23	3.12	4.09	3.72	4.03	3.98	3.92	5.11	2.70	4.10	2.89	4.57	4.54
Eu	1.12	1.40	1.16	1.02	1.04	1.23	1.28	1.03	1.43	1.50	1.45	1.18	1.29	1.65	0.75	1.32	0.78	1.09	1.13
Gd	3.16	3.77	2.81	2.52	2.45	2.86	2.85	2.72	3.68	3.32	3.59	3.43	3.55	4.38	2.51	3.81	2.58	4.05	4.06
Tb	0.63	0.81	0.58	0.48	0.48	0.51	0.51	0.54	0.80	0.60	0.65	0.68	0.65	0.78	0.44	0.65	0.48	0.76	0.75
Dy	3.72	5.19	3.52	2.73	2.77	2.91	2.90	3.26	4.99	3.39	3.72	4.04	3.75	4.46	2.40	3.62	2.74	4.34	4.30
Ho	0.75	1.10	0.73	0.55	0.57	0.59	0.59	0.65	1.03	0.69	0.74	0.85	0.77	0.90	0.46	0.72	0.56	0.88	0.87
Er	2.09	3.00	1.94	1.56	1.52	1.59	1.59	1.71	2.70	1.92	2.11	2.29	2.10	6.58	1.23	1.97	1.53	2.43	2.36
Tm	0.33	0.51	0.32	0.24	0.24	0.27	0.27	0.28	0.45	0.30	0.34	0.38	0.34	0.42	0.20	0.33	0.26	0.42	0.39
Yb	2.24	3.46	2.16	1.55	1.65	1.87	1.87	1.92	3.09	2.08	2.29	2.63	2.40	2.93	1.37	2.29	1.85	2.95	2.79
Lu	0.34	0.53	0.32	0.23	0.25	0.28	0.28	0.29	0.46	0.31	0.34	0.39	0.36	0.45	0.21	0.35	0.28	0.46	0.43
(La/Yb)N	3.61	2.19	2.75	3.73	4.05	6.58	6.06	3.13	2.09	5.43	5.40	3.69	5.34	5.71	6.30	7.00	5.41	4.88	5.18
(Gd/Yb)N	1.17	0.90	1.08	1.34	1.23	1.27	1.26	1.17	0.99	1.32	1.30	1.08	1.22	1.24	1.51	1.38	1.15	1.14	1.20
Eu/Eu*	1.01	1.10	1.16	1.18	1.20	1.21	1.28	1.08	1.13	1.30	1.17	0.98	1.05	1.07	0.88	1.02	0.87	0.77	0.80
ΣREE	77	76	62	61	63	77	78	60	71	84	96	86	99	133	73	121	76	110	120

Note: CIA=[Al$_2$O$_3$/(Al$_2$O$_3$+CaO*+Na$_2$O+K$_2$O)]×100 and PIA=[(Al$_2$O$_3$–K$_2$O)/(Al$_2$O$_3$+CaO*+Na$_2$O–K$_2$O)]×100, where CaO* represents Ca in silicate-bearing minerals only and all in molecular proportions; ICV= (Fe$_2$O$_3$+K$_2$O+Na$_2$O+CaO+MgO+TiO$_2$)/Al$_2$O$_3$.

Table 2. Sr-Nd isotopic composition of the Carboniferous turbidites in the NTAC

Sample	$^{87}Rb/^{86}Sr$	$^{87}Sr/^{86}Sr$	2σ	$(^{87}Sr/^{86}Sr)i$	$^{147}Sm/^{144}Nd$	$^{143}Nd/^{144}Nd$	2σ	$(^{143}Nd/^{144}Nd)i$	$\varepsilon Nd(t)$	T^1_{DM}	T^2_{DM}
TS17-11	0.103248	0.705150	0.000006	0.704695	0.142028	0.512898	0.000007	0.512610	7.2	540	482
TS17-13	0.120980	0.705748	0.000006	0.705214	0.143956	0.512880	0.000005	0.512588	6.8	594	517
TS17-38	0.145475	0.705022	0.000006	0.704380	0.149295	0.512931	0.000006	0.512628	7.6	522	453
TS17-49	0.147287	0.704963	0.000008	0.704313	0.163533	0.512975	0.000005	0.512643	7.9	537	429
TS17-67	0.164843	0.706159	0.000006	0.705432	0.129772	0.512782	0.000008	0.512519	5.5	672	627
TS17-71	0.152381	0.705974	0.000005	0.705302	0.129367	0.512543	0.000006	0.512280	0.8	1100	1006

Unit of model age (T^1_{DM} and T^2_{DM}) is Ma.

$\varepsilon_{Nd}(t)=[[(^{143}Nd/^{144}Nd)_S/(^{143}Nd/^{144}Nd)_{CHUR}-1]\times10,000$.

$T^1_{DM}=1/\lambda_{Sm}\times ln\{[(^{143}Nd/^{144}Nd)_S-0.51315]/[(^{147}Sm/^{144}Nd)_S-0.2137]\}$.

$T^2_{DM}=T^1_{DM}-(T^1_{DM}-t)\times[(f_{CC}-f_S)/(f_{CC}-f_{DM})]$.

where S= sample, $(^{143}Nd/^{144}Nd)_{CHUR}=0.512638$ and $(^{147}Sm/^{144}Nd)_{CHUR}=0.1967$. The f_{CC}, f_S and f_{DM} are $f_{Sm/Nd}$ values of the continental crust, the sample and the depleted mantle, respectively.
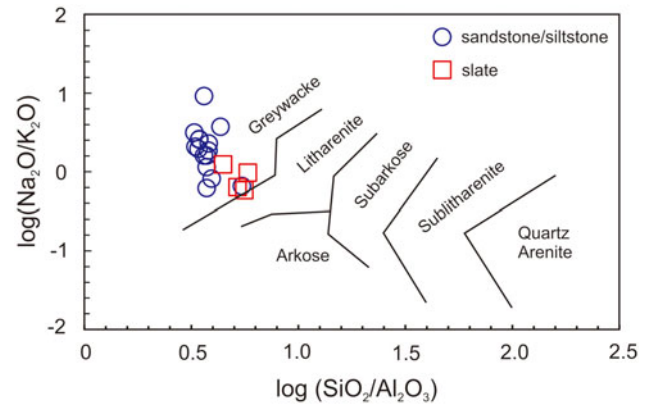
Figure 4. (Colour online) Geochemical classification diagram of the turbidites in the NTAC (after Herron, 1988).

siltstones have SiO_2/Al_2O_3 ratios of 3.3–5.5, indicating low degree and sorting and deposition close to sources. The slates have slightly higher SiO_2/Al_2O_3 ratios of 4.4–5.8, suggesting possibly stronger weathering.

To conclude, the turbidites from the NTAC were first cycle sediments and derived from immature materials with low degree of chemical weathering. The slates might contain hither contents of materials which experience slightly stronger weathering than the sandstone/siltstone samples.

5.b. Source rocks and tectonic setting

The turbidites from the NTAC are characterized by large proportions of angular volcanic lithic fragments and immature geochemical signatures, suggesting that they were derived from a nearby magmatic arc. The sandstone/siltstone samples have more mafic to andesitic volcanic clasts than the slates, indicating a more mafic source. This is consistent with the geochemical data. Geochemical characteristics of sedimentary rocks derived from different source rocks have been studied for a long time (Bhatia and Taylor, 1981; Bhatia and Crook, 1986; McLennan and Taylor, 1991; Safonova *et al.* 2022a, b). According to the source rock discrimination diagrams using major elements (Fig. 8a), the sandstone/siltstone from the NTAC were mainly derived from intermediate and felsic igneous rocks, while the slates were mainly from felsic igneous rocks and quartz-rich sedimentary rocks. In the La/Th versus Hf diagram (Fig. 8b), most sandstone/siltstone samples plot in the mixed felsic/basic source area, while the slates plot in the acid arc source area. Potassium and Rb are relatively mobile elements during low grade metamorphism and diagenesis, but their covariant relation is generally considered as a standard for determining the source rocks of clastic rocks (Floyd *et al.* 1989). Although the samples from the NTAC show a wide range of K/Rb ratios, their high Rb and K_2O contents indicate the derivation from acidic to intermediate igneous rocks (Fig. 8c). Some trace element ratios, such as Th/Sc, Co/Th, La/Sc, and Ti/Zr are also good indicators for provenance study, as silicic rocks trends to have more contents of Th and Zr, whereas basic rocks hold more contents of Sc, Co, and Ti (Cullers, 1994). Th/Sc and Zr/Sc ratios increase with supply of felsic detritus, whereas Ti/Zr and Co/Th ratios decrease. Most of the sandstone/siltstones have higher Ti/Zr ratios (12.4–83.3, av. = 39.5) compared to the UCC (19.9), indicating dominantly basic-intermediate igneous rocks in the source area. In comparison, the slates exhibit relatively low Ti/Zr
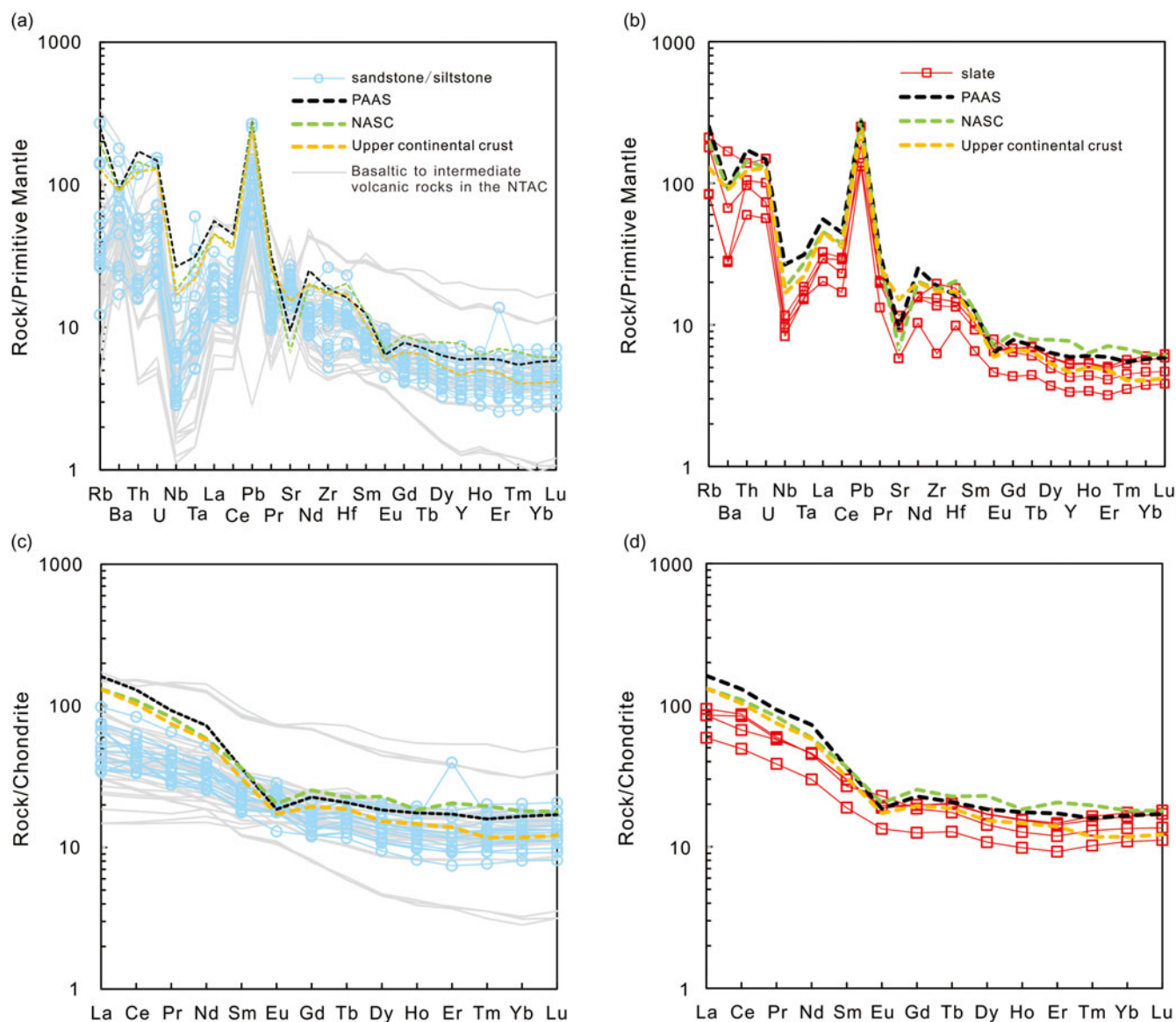
Figure 5. (Colour online) Chondrite-normalized REE patterns and upper crust-normalized spider diagrams for the Paleozoic graywackes. Symbols are the same as in Fig. 4. Chondrite and PM normalizing values are from Sun and McDonough (1989) and upper crust-normalizing data are from Taylor and McLennan (1985). Geochemical data for volcanic rocks in the NTAC are from Liu *et al.* (2012), Wang *et al.* (2017) and Bai *et al.* (2020).

ratios (15.6–35.1, av. = 20.2), suggesting a dominantly felsic igneous source. In the Co/Th versus La/Sc diagrams (Fig. 8d), the sandstone/siltstone samples plot in a mixing source from basalt to andesite and felsic volcanic rocks. As a contrast, the slates mainly distribute around the felsic rocks (Fig. 8d). These features indicate a provenance of basaltic to felsic rocks for the sandstone/siltstones and mainly felsic rocks for the slates.

The major and trace element compositions of sediments are also widely used to constrain the tectonic setting of their source rocks (Bhatia and Taylor, 1981; Roser and Korsch, 1986; Bhatia and Crook, 1986). Generally, sandstones sourced from oceanic island arcs the have higher $Fe_2O_3^T + MgO$, Al_2O_3, and TiO_2, and lower SiO_2, K_2O/Na_2O, and $Al_2O_3/(Na_2O + CaO)$ than those sourced from passive margins (Bhatia, 1983). In the K_2O/Na_2O

versus $Fe_2O_3^T + MgO$, $Al_2O_3/(Na_2O + CaO)$ versus $Fe_2O_3^T + MgO$, TiO_2 versus $Fe_2O_3^T + MgO$, and Al_2O_3/SiO_2 versus $Fe_2O_3^T + MgO$ diagrams (Fig. 9a-d), the sandstone/siltstones all plot within or near the oceanic island arc and continental island arc fields, while the slates mainly distribute within or around the active continental margin field. When plotting on the Df1 versus Df2 diagram which considers the role of multiple variables (Fig. 9e), it shows that the sandstone/siltstones illustrate an oceanic island and active continental margin setting, while the slates reflect an active continental margin setting. In the $(Fe_2O_3^T + MgO)/(SiO_2 + Na_2O + K_2O)$ versus Al_2O_3/SiO_2 diagram (Fig. 9f), most of the sandstone/siltstone samples fall within the immature island arc (IIA) field and evolved island arc (EIA) field, while the slates mainly fall within the mature magmatic arc (MMA) field. Similar
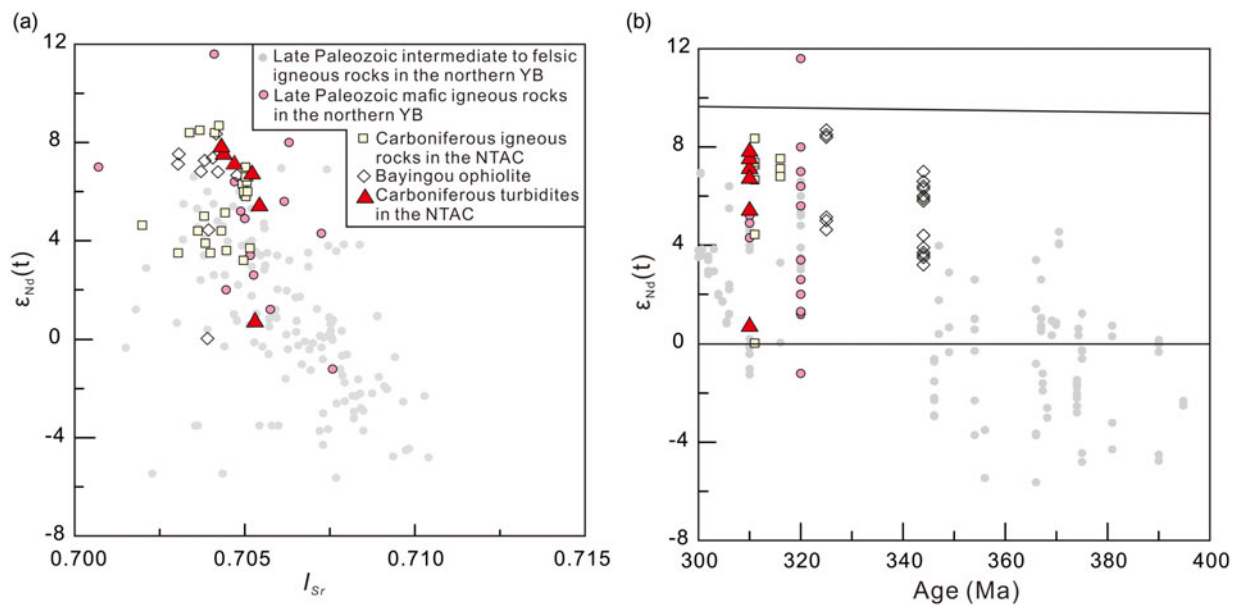
Figure 6. (Colour online) εNd(t) versus age diagram for the Paleozoic igneous rocks and sediments in the northern Chinese West Tianshan. Nd isotopic Data for the igneous rocks can be found in Supplementary Table S1.
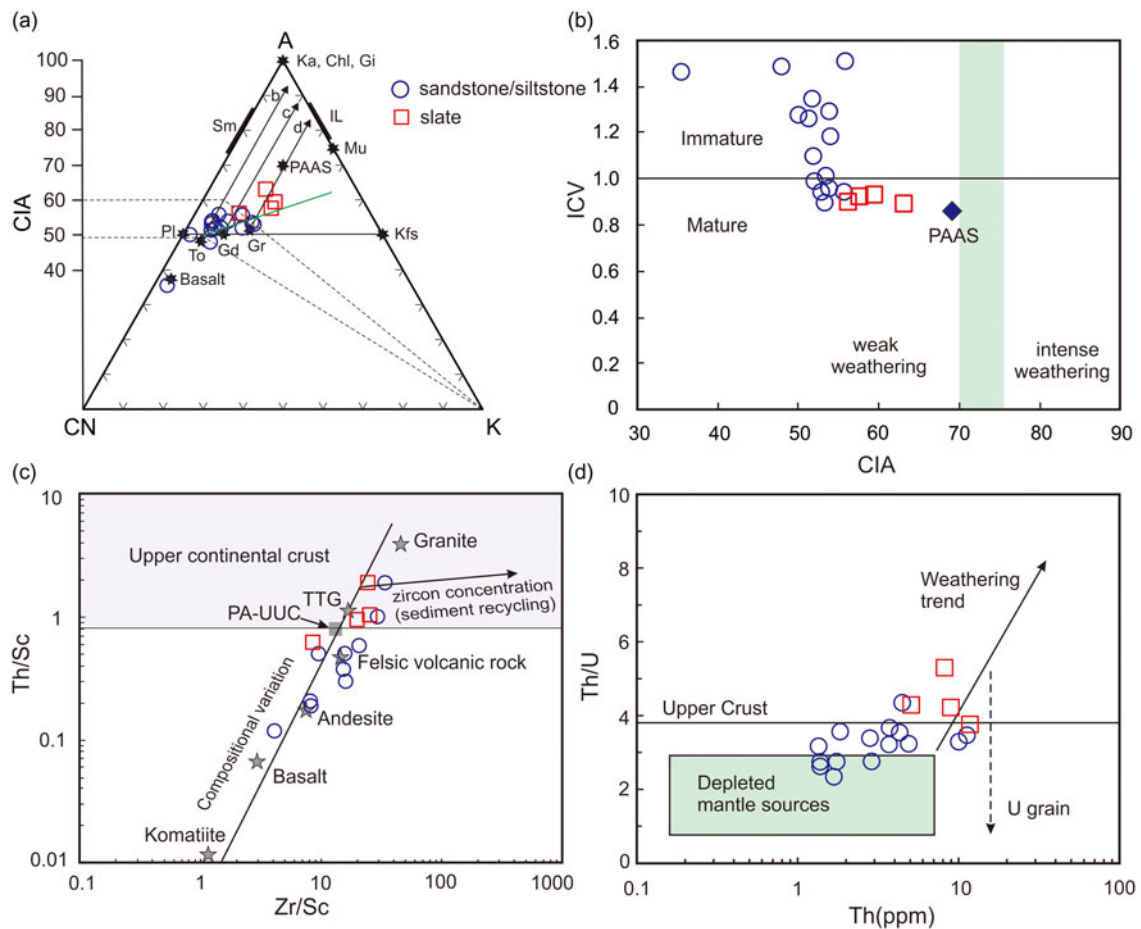

Figure 7. (Colour online) Discrimination diagrams illustrating weathering and sediment recycling. (a) Th/Sc versus Zr/Sc diagram (after McLennan *et al.* 1993); (b) A-CN-K diagram (after Fedo *et al.* 1995), Data for basalt (Ba) tonalite (To), granodiorite (Gd), granite (Gr), and average post-Archean upper crust are from Condie (1993) and Nesbitt and Young (1984); (c) Th/U versus Th (after McLennan *et al.* 1993); (d) ICV versus CIA diagram (after Nesbitt and Young, 1984).
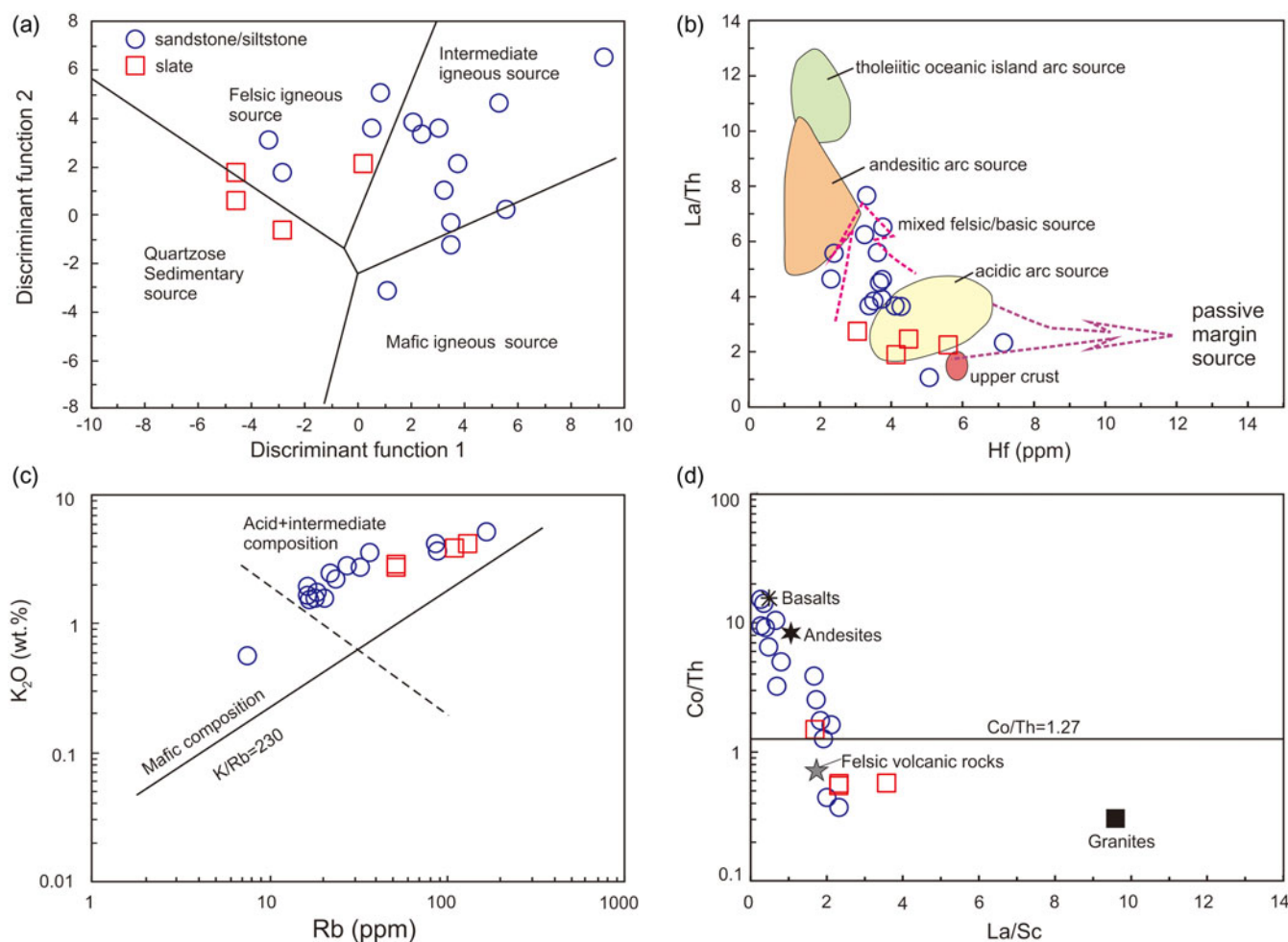
Figure 8. (Colour online) Source rock discrimination diagrams. (a) discriminant function diagram using major elements after Roser and Korsch (1988); (b) La/Th versus Hf diagram (after Floyd and Leveridge, 1987); (c) K₂O versus Rb diagram (after Folyd *et al.* 1989); (d) Co/Th versus La/Sc diagram (after Gu *et al.* 2002).
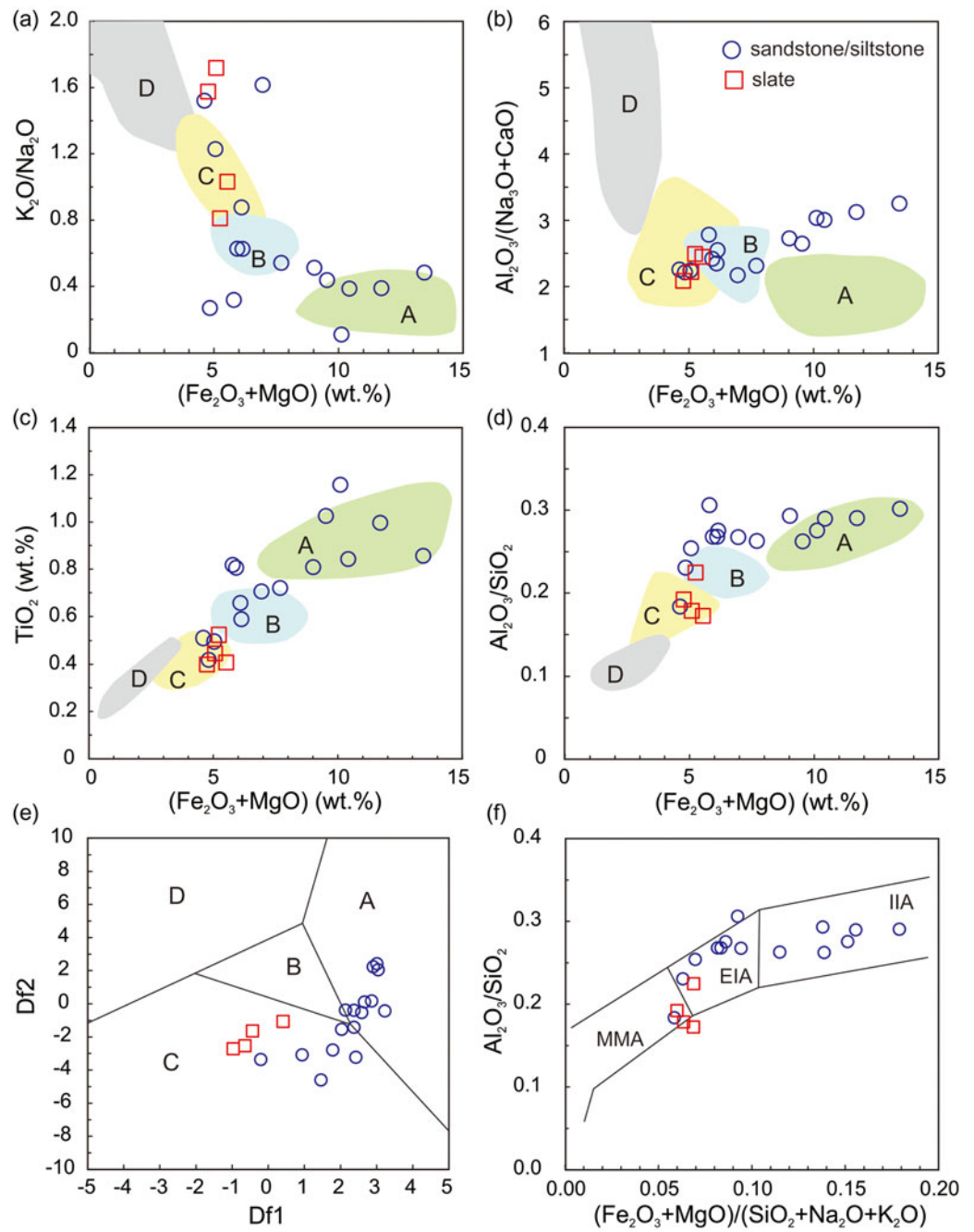
results are observed in the tectonic setting discrimination diagrams using trace elements (Fig. 10).

In the northern YB and the NTAC, there are massive Paleozoic volcanic and intrusive rocks which exhibit distinguishable Nd isotope characteristics (Fig. 6). The sandstone/siltstone samples have comparable Sr-Nd isotope compositions with the Late Paleozoic mafic igneous rocks in the northern YB and Carboniferous volcanic rocks in the NTAC (Fig. 6). If they were mainly sourced from the northern YB, their source rocks were supposed to contain the felsic volcanic rocks as these rocks make up a larger proportion in the northern YB (Fig. 1b). This is inconsistent with the above suggestion that the source rocks of the sandstone/siltstones are mainly basic-intermediate igneous rocks. In addition, the U-Pb ages of the turbidites are unimodal with major peaks at 323 Ma (Fig. 11a; Wang *et al.* 2018a). It is completely different from the detrital zircon age spectrum of Early Carboniferous sandstone just to the south of the North Tianshan Fault, which contain many Early Paleozoic and Precambrian detrital zircons (Wang *et al.* 2018c). What is more, the sandstone/ siltstones from the NTAC have depleted whole-rock Nd isotope and detrital zircon Hf isotope composition (Fig. 6 and Fig. 11b),

indicating a juvenile mantle source for their parental rocks, which might be part of an intra-oceanic arc. These features indicate the sandstone/siltstone were sourced from a Carboniferous intra-oceanic arc and deposited in a fore-arc/trench. The source rocks of the slate are more felsic and might be part of a continental arc. Therefore, the turbidites from the NTAC were likely deposited between an intra-oceanic arc (the North Tianshan arc) and a continental arc (the northern YB).

5.c. Implication for crustal growth in the CAOB

Juvenile continental growth can be recorded by trondhjemite-granodiorite (TTG) and mafic magmatism at supra-subduciton zone and intra-plate settings (Safonova, 2017). However, the oceanic crust was mostly subducted into deep mantle and the intra-oceanic arcs could have been eroded or buried deeply in the lower crust, which might lead to the underestimation of proportion of juvenile crust. Turbidites and greywackes deposited at convergent margin are sourced from upper crust of the adjacent plates and thus recorded the nature of these upper crust rocks. If these sediments were sourced from the juvenile materials, then it represents continental

Figure 9. (Colour online) Tectonic setting discrimination diagrams using major elements for turbidites in the NTAC (after Bhatia, 1983; Kumon and Kiminami, 1994). (a) K_2O/Na_2O versus $(Fe_2O_3+ MgO)$ diagram; (b) $Al_2O_3/(Na_2O + CaO)$ versus $(Fe_2O_3+ MgO)$ diagram; (c) TiO_2 versus $(Fe_2O_3+ MgO)$ diagram; (d) Al_2O_3/SiO_2 versus $(Fe_2O_3+ MgO)$ diagram; (e) Df1 versus Df2 diagram; (f) Al_2O_3/SiO_2 versus $(Fe_2O_3+ MgO)/(SiO_2+ Na_2O + K_2O)$ diagram. The discriminant functions are: $Df1 = -0.0447 \times SiO_2 - 0.972 \times TiO_2 + 0.008 \times Al_2O_3 - 0.267 \times Fe_2O_3 + 0.208 \times FeO - 3.082 \times MnO + 0.14 + MgO + 0.195 \times CaO + 0.719 \times Na_2O - 0.032 \times K_2O + 7.510 \times P_2O_5 + 0.303$; $Df2 = -0.421 \times SiO_2 + 1.988 \times TiO_2 - 0.526 \times Al_2O_3 - 0.551 \times Fe_2O_3 - 1.61 \times FeO + 2.72 \times MnO + 0.881 \times MgO - 0.907 \times CaO - 0.177 \times Na_2O - 1.84 \times K_2O + 7.244 \times P_2O_5 + 43.57$. Abbreviations for tectonic settings: A, oceanic island arc; B, continental arc; C, active continental margin; D, passive continental margin; IIA, immature island arc; EIA, evolved island arc; MMA, mature magmatic arc.

growth (Kröner *et al.* 2017). Recent geochemical, detrital zircon geochronological and Hf-Nd isotopic studies on sandstones from central and eastern Kazakhstan had implied several pre-existed intra-oceanic arcs (Safonova *et al.* 2022a, b).

Though the outcrop is limited, the occurrence of Carboniferous arc type volcanic rocks in the NTAC, and juvenile source nature of the turbidites allow us to infer that there was a Late Devonian to Carboniferous intra-oceanic arc to the north of the YB, which was partly eroded and/or covered later. Here, we term this intra-oceanic arc as the North Tianshan arc, also

mentioned by Bai *et al.* (2020). However, the extent of the North Tianshan arc was unknown, maybe equivalently to the NTAC, because most of this arc was overlain by the Carboniferous turbidites. Another evidence for the arc nature of the NTAC basement is the magnetic anomaly data in the northern Xinjiang (He *et al.* 2013). To the east of Urumqi, the Bogda Range contains massive Carboniferous magmatic rocks with geochemical signatures of oceanic island arc and was called the Bogda arc (Xie *et al.* 2016; Memtimin *et al.* 2020). According to the magnetic anomaly data, the Bogda arc is characterized by a medium–low
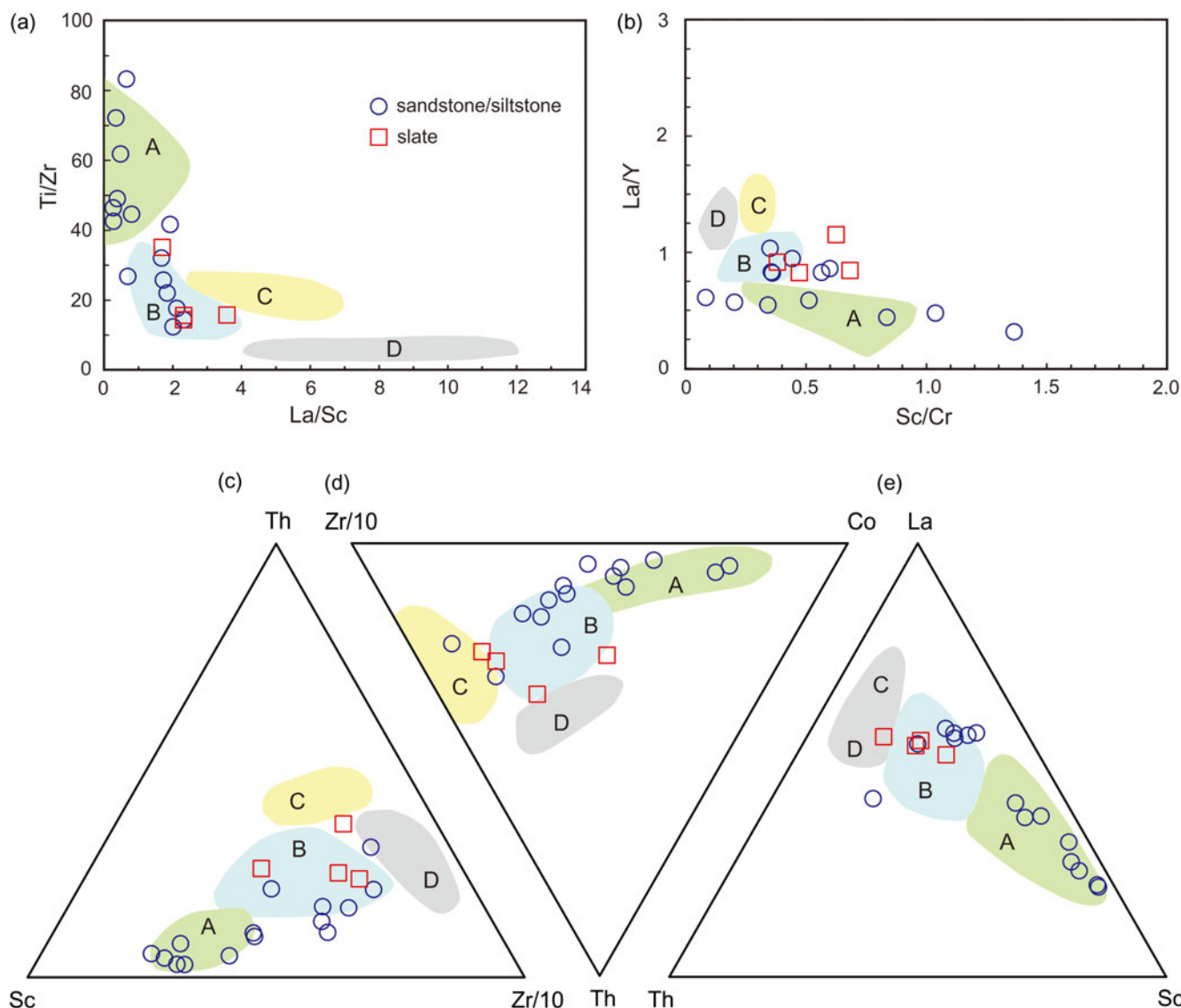
Figure 10. (Colour online) Tectonic setting discrimination diagrams using trace elements for turbidites in the NTAC (after Bhatia and Crook, 1986). (a) Ti/Zr versus La/Sc diagram; (b) La/Y versus Sc/Cr; (c) Th-Sc-Zr/10 diagram; (d) Th-Co-Zr/10 diagram; (e) La-Th-Sc diagram. Abbreviations for tectonic settings are the same as in Fig. 9.

magnetic anomaly, and this anomaly extends westward to the North Tianshan area (He *et al.* 2013). This similarity suggests that the basement of the NTAC (the North Tianshan arc) might be linked with the Bogda arc. The Late Carboniferous Arbasay Formation may represent limited outcrop of the North Tianshan arc (Bai *et al.* 2020).

In summary, our study indicates the possibly pre-existence of a Devonian to Carboniferous intra-oceanic arc, i.e., the North Tianshan arc, to the north or the YB. This arc was then partly eroded and transferred to form the Carboniferous turbidites with overlain sequences. This study further proves the validity of using sedimentary record to reveal neglected juvenile crustal growth in accretionary orogens. The contribution of the eroded or covered intra-oceanic arc should be considered when calculating the net crustal growth in the CAOB.

6. Conclusions

(1) The turbidites in the North Tianshan Accretionary Complex are mainly composed of sandstone, siltstone and slate, and belong to greywackes.

(2) The sandstone and siltstone are characterized by immature geochemical features suggesting derivation from mafic to intermediate volcanic rocks, while the slates from a felsic magmatic source.

(3) The sandstone and siltstone display high positive εNd(t) values (+5.5 to +7.9) with only one exception of +0.8, implying derivation from juvenile crust rocks. Combining with previous studies, we suggest that the basement of the North Tianshan might be a Devonian to Carboniferous intra-oceanic arc.
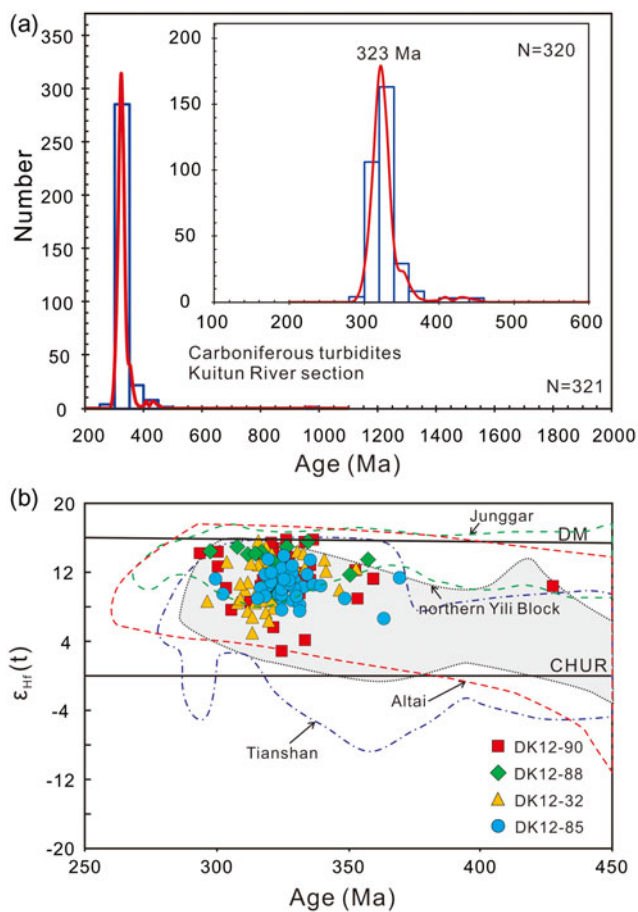
Figure 11. (Colour online) (a) Relative probability plot for detrital zircons from turbidites in the NTAC (after Wang *et al.* 2018a); (b) Plot of εHf(t) versus U-Pb age for detrital zircons from turbidites in the NTAC (after Wang *et al.* 2018a).

References

Bai XY, Chen YC, Song DF, Xiao WJ, Windley BF, Ao SJ, Li L and Xiang DF (2020). A new Carboniferous–Permian intra-oceanic subduction system in the North Tianshan (NW China): implications for multiple accretionary tectonics of the southern Altaids. *Geological Journal* **55**, 2232–53.

Bhatia MR (1983) Plate-tectonics and geochemical composition of sandstones. *Journal of Geology* **91**, 611–627.

Bhatia MR and Crook KAW (1986) Trace element characteristics of graywackes and tectonic setting discrimination of sedimentary basins. *Contributions to Mineralogy and Petrology* **92**, 181–193.

Bhatia MR and Taylor SR (1981) Trace-element geochemistry and sedimentary provinces: a study from the Tasman geosyncline, Australia. *Chemical Geology* **33**, 115–125.

Briqueu L, Bougault H and Joron JL (1984) Quantification of Nb, Ta, Ti and V anomalies in magmas associated with subduction zones: petrogenetic implications. *Earth and Planetary Science Letters* **68**, 297–308.

Charvet J, Shu LS, Laurent-Charvet S, Wang B, Faure M, Cluzel D, Chen Y and De Jong K (2011) Palaeozoic tectonic evolution of the Tianshan Belt, NW China. *Science China: Earth Sciences* **54**, 166–184.

Condie KC (1993) Chemical composition and evolution of the upper continental crust: contrasting results from surface samples and shales. *Chemical Geology* **104**, 1–37.

Cox R and Lowe DR (1995) A conceptual review of regional-scale controls on the composition of clastic sediment and the co-evolution of continental blocks and their sedimentary cover. *Journal of Sedimentary Research* **1**, 1–12.

Cullers RL (1994) The chemical signature of source rocks in size fractions of Holocene stream sediment derived from metamorphic rocks in the Wet Mountains region, Colorado, U.S.A. *Chemical Geology* **113**, 327–343.

Dong YP, Zhang GW, Neubauer F, Liu XM, Hauzenberger C, Zhou DW and Li W (2011) Syn- and post-collisional granitoids in the Central Tianshan orogen: geochemistry, geochronology and implications for tectonic evolution. *Gondwana Research* **20**, 568–581.

Fedo CM, Nesbitt HW and Young GM (1995). Unraveling the effects of potassium metasomatism in sedimentary rocks and paleosoils, with implications for paleoweathering conditions and provenance. *Geology* **23**, 921–924

Feng WY and Zhu YF (2018) Petrology and geochemistry of mafic and ultramafic rocks in the north Tianshan ophiolite: implications for petrogenesis and tectonic setting. *Lithos* **318–319**, 124–142.

Floyd PA and Leveridge BE (1987) Tectonic environment of the Devonian Gramscatho basin, south Cornwall: framework mode and geochemical evidence from turbiditic sandstones. *Journal of the Geological Society* **144**, 531–542.

Floyd PA, Winchester JA and Park RG (1989) Geochemistry and tectonic setting of Lewisian clastic metasediments from the Early Proterozoic Loch Maree Group of Gairloch, NW Scotland. *Precambrian Research* **45**, 203–214.

Gao J, He GQ and Li MS (1995) The mineralogy, petrology, metamorphic PTDt trajectory and exhumation mechanism of blueschists, south Tianshan, northwestern China. *Tectonophysics* **250**, 151–168.

Gao J, Long LL, Klemd R, Qian Q, Liu DY, Xiong XM, Su W, Liu W, Wang YT and Yang FQ (2009) Tectonic evolution of the South Tianshan Orogen and adjacent regions, NW China: geochemical and age constraints of granitoid rocks. *International Journal of Earth Sciences* **98**, 1221–1238.

Gao J, Wang XS, Klemd R, Jiang T, Qian Q, Mu LX and Ma YZ (2015) Record of assembly and breakup of Rodinia in the Southwestern Altaids: evidence from Neoproterozoic magmatism in the Chinese Western Tianshan Orogen. *Journal of Asian Earth Sciences* **113**, 173–193.

Gu XX, Liu JM, Zheng MH, Tang JX and Qi L (2002). Provenance and tectonic setting of the Proterozoic turbidites in Hunan, south China: geochemical evidence. *Journal of Sedimentary Research* **72**, 393–407

Han BF, Guo ZJ, Zhang ZC, Zheng L, Chen J and Song B (2010) Age, geochemistry, and tectonic implications of a late Paleozoic stitching pluton in the North Tian Shan suture zone, western China. *Geological Society of America Bulletin* **122**, 627–640.

He DF, Li D, Fan C and Yang XF (2013) Geochronology, geochemistry and tectonostratigraphy of Carboniferous strata of the deepest well Moshen-1 in the Junggar Basin, Northwest China: insights into the continental growth of Central Asia. *Gondwana Research* **24**, 560–577.

Hegner E, Klemd R, Kröner A, Corsini M, Alexeiev DV, Iaccheri LM, Zack T, Dulski P, Xia X and Windley BF (2010) Mineral ages and P-T conditions of Late Paleozoic high-pressure eclogite and provenance of mélange sediments from Atbashi in the south Tianshan orogen of Kyrgyzstan. *American Journal of Science* **310**, 916–950.

Herron MM (1988) Geochemical classification of terrigenous sands and shales from core or log data. *Journal of Sedimentary Research* **58**, 820–829.

Hu AQ, Wei GJ, Jahn BM, Zhang JB, Deng WF and Chen LL (2010) Formation of the 0.9 Ga Neoproterozoic granitoids in the Tianshan Orogen, NW China: constraints from the SHRIMP zircon age determination and its tectonic significance. *Geochimica* **39**, 197–212.

Huang H, Cawood PA, Ni SJ, Hou MC, Shi ZQ and Hu XL (2017) Provenance of late Paleozoic strata in the Yili Basin: implications for tectonic evolution of the south Tianshan orogenic belt. *Geological Society of America Bulletin* **130**, 952–974.

Huang H, Wang T, Tong Y, Qin Q, Ma XX and Yin JY (2020) Rejuvenation of ancient micro-continents during accretionary orogenesis: insights from the Yili Block and adjacent regions of the SW Central Asian Orogenic Belt. *Earth Science Review* **208**, 103255.

Huang ZY, Long XP, Kröner A, Yuan C, Wang Q, Sun M, Zhao GC and Wang YJ (2013) Geochemistry, zircon U-Pb ages and Lu-Hf isotopes of early Paleozoic plutons in the northwestern Chinese Tianshan: petrogenesis and geological implications. *Lithos* **182**, 48–66.

Jahn BM., Windley B, Natal'in B and Dobretsov N (2004) Phanerozoic continental growth in Central Asia. *Journal of Asian Earth Sciences* **23**, 599–603.

Jahn BM, Wu FY and Chen B (2000) Granitoids of the Central Asian Orogenic Belt and continental growth in the Phanerozoic. *Earth and Environmental Science Transactions of the Royal Society of Edinburgh* **91**, 181–193.

Jiang T, Gao J, Klemd R, Qian Q, Zhang X, Xiong XM, Wang XS, Tan Z and Chen BX (2014) Paleozoic ophiolitic mélanges from the South Tianshan Orogen, NW China: geological, geochemical and geochronological implications for the geodynamic setting. *Tectonophysics* **612–613**, 106–127.

Jin HJ, Li YC and Li JY (1989) The flysch facies of Middle Carboniferous in the Northern Tianshan, Xinjiang. *Acta Sedimentologica Sinica* **7**, 49–59.

Kröner A, Kovach V, Alexeiev D, Wang KL, Wong J, Degtyarev K and Kozakov I (2017) No excessive crustal growth in the Central Asian Orogenic Belt: further evidence from field relationships and isotopic data. *Gondwana Research* **50**, 135–166.

Kröner A, Kovach V, Belousova E, Hegner E, Armstrong R, Dolgopolova A, Seltmann R, Alexeiev DV, Hofmann JE, Wong J, Sun M, Cai KD, Wang T, Tong Y, Wilde SA, Degtyarev KE and Rytsk E (2014) Reassessment of continental growth during the accretionary history of the Central Asian Orogenic Belt. *Gondwana Research* **25**, 103–125

Kumon F and Kiminami K (1994) Modal and chemical compositions of the representative sandstones from the Japanese Islands and their tectonic implications. In Proceedings of the 29th International Geological Congress: Part A, p. 135–151

Li C, Xiao WJ, Han CM, Zhou KF, Zhang JE and Zhang ZX (2015) Late Devonian–early Permian accretionary orogenesis along the North Tianshan in the southern Central Asian Orogenic Belt. *International Geology Review* **57**, 1023–1050.

Li CF, Li XH, Li QL, Guo JH and Yang YH (2012). Rapid and precise determination of sr and nd isotopic ratios in geological samples from the same filament loading by thermal ionization mass spectrometry employing a single-step separation scheme. *Analytica Chimica Acta*, **727**, 54–60.

Li J, Tang SH, Zhu XK and Pan CX (2017). Production and Certification of the Reference Material GSB 04-3258-2015 as a $^{143}Nd/^{144}Nd$ Isotope Ratio Reference. *Geostandards and Geoanalytical Research* **41**, 255–262.

Liu DD, Cheng F, Guo ZJ, Jolivet M and Song Y (2015) Lahar facies of the Latest Paleozoic Arbasay Formation: geomorphological characters and paleoenvironment reconstruction of Northern Tian Shan, NW China. *Journal of Asian Earth Sciences* **113**, 282–292.

Liu DD, Guo ZJ, Zhang ZC and Wu CD (2012) The Late Paleozoic tectonic relationship between the Tian Shan orogenic belt and Junggar basin: Constraints from zircon SHRIMP U-Pb dating and geochemistry characteristics of volcanic rocks in Arbasay Formation. *Acta Petrologica Sinica* **28**, 2355–2368.

Long XP and Huang ZY (2017) Tectonic affinities of microcontinents in the Central Asian Orogenic Belt: a case study of the Chinese Tianshan Orogenic Belt. *Bulletin of Mineralogy, Petrology and Geochemistry* **36**, 771–785.

McLennan SM, Hemming S, Mcdaniel DK and Hanson GN (1993) Geochemical approaches to sedimentation, provenance, and tectonics. *Geological Society of America Bulletin* **284**, 21–40.

McLennan SM and Taylor SR (1991) Sedimentary-Rocks and Crustal Evolution: tectonic Setting and Secular Trends. *Journal of Geology* **99**, 1–21.

Memtimin M, Pe-Piper G, Piper DJW, Guo ZJ and Zhang YY (2020) Carboniferous arc-related volcanism in SW Bogda Mountain, Northwest China, and its implications for regional tectonics. *Lithos* **360–361**, 105413.

Nesbitt HW and Young GM (1984) Prediction of some weathering trends of plutonic andvolcanic rocks based on thermodynamics and kinetic considerations. *Geochimica et Cosmochimica Acta* **48**, 1523–1534.

Roser BP, Cooper RA, Nathan S and Tulloch AJ (1996) Reconnaissance sandstone geochemistry, provenance, and tectonic setting of the lower Paleozoic terranes of the West Coast and Nelson, New Zealand. *New Zealand Journal of Geology and Geophysics* **39**, 1–16.

Roser BP and Korsch RJ (1986) Determination of Tectonic Setting of Sandstone-Mudstone Suites Using SiO_2 Content and K_2O/Na_2O Ratio. *Journal of Geology* **94**, 635–650.

Roser BP and Korsch RJ (1988) Provenance signatures of sandstone-mudstone suite determined using discrimination function analysis of major-element data. *Chemical Geology* **67**, 119–139.

Safonova I (2017) Juvenile versus recycled crust in the Central Asian Orogenic Belt: implications from ocean plate stratigraphy, blueschist belts and intra-oceanic arcs. *Gondwana Research* **47**, 6–27.

Safonova I, Perfilova A, Obut O, Kotler P, Aoki S, Komiya T, Wang B and Sun M (2022b) Traces of intra-oceanic arcs recorded in sandstones of eastern Kazakhstan: implications from U–Pb detrital zircon ages, geochemistry, and Nd–Hf isotopes. *International Journal of Earth Sciences* **111**, 2449–2468.

Safonova I, Perfilova A, Savinskiy I, Kotler P, Sun M and Wang B (2022a) Sandstones of the Itmurundy accretionary complex, central Kazakhstan, as archives of arc magmatism and subduction erosion: evidence from U-Pb zircon ages, geochemistry and Hf-Nd isotopes. *Gondwana Research* **111**, 35–52.

Şengör AMC, Natal'in BA and Burtman US (1993) Evolution of the Altaid tectonic collage and Paleozoic crustal growth in Eurasia. *Nature* **364**, 209–304.

Sun SS and McDonough WF (1989) Chemical and isotopic systematics of oceanic Basalts: implications for mantle composition and processes. *Geological Society, London Special Publications* **42**, 313–45

Taylor SR and McLennan SM (1985) *The Continental Crust: Its Composition and Evolution.* Oxford, UK: Blackwell Scientific Publications, pp. 312

Taylor SR, McLennan SM, Armstrong RL and Tarney J (1981) The composition and evolution of the continental crust: rare earth element evidence from sedimentary rocks. *Philosophical Transactions of the Royal Society A: Mathematical, Physical and Engineering Sciences* **301**, 381–399.

Van de KPC and Leake BE (1985) Petrography and geochemistry of feldspathic and mafic sediments of the northeastern Pacific margin. *Earth and Environmental Science Transactions of The Royal Society of Edinburgh* **76**, 411–449.

Wang B, Faure M, Cluzel D, Shu LS, Charvet J, Meffre S and Ma Q (2006) Late Paleozoic tectonic evolution of the northern West Tianshan, NW China. *Geodinamica Acta* **19**, 237–247.

Wang B, Jahn BM, Shu LS, Li KS, Chung SL and Liu DY (2012) Middle-Late Ordovician arc-type plutonism in the NW Chinese Tianshan: implication for the accretion of the Kazakhstan continent in Central Asia. *Journal of Asian Earth Sciences* **49**, 40–53.

Wang B, Liu HS, Shu LS, Jahn BM, Chung SL, Zhai YZ and Liu DY (2014) Early Neoproterozoic crustal evolution in northern Yili block: insights from migmatite, orthogneiss and leucogranite of the Wenquan metamorphic complex in the NW Chinese Tianshan. *Precambrian Research* **242**, 58–81.

Wang B, Shu LS, Faure M, Jahn BM, Cluzel D, Charvet J, Chung SL and Meffre S (2011) Paleozoic tectonics of the southern Chinese Tianshan: insights from structural, chronological and geochemical studies of the Heiyingshan ophiolitic mélange (NW China). *Tectonophysics* **497**, 85–104

Wang B, Zhai YZ, Kapp P, de Jong K, Zhong LL, Liu HS, Ma YZ, Gong HJ and Geng H (2018b) Accretionary tectonics of back-arc oceanic basins in the South Tianshan: insights from structural, geochronological, and geochemical studies of the Wuwamen ophiolite mélange. *Geological Society of America Bulletin* **130**, 284–306.

Wang JL, Wu CD, Li Z, Zhu W, Chen YW, Li QY, Wu J, Deng LJ and Chen L (2017) Geochronology and geochemistry of volcanic rocks in the Arbasay Formation, Xinjiang Province (Northwest China): implications for the tectonic evolution of the North Tianshan. *International Geology Review* **59**, 1324–1343.

Wang M, Zhang B, Ren R, Pei XZ, Zhang JJ, Chen YX, Li ZC and Ge MH (2022) Tracing tectonic processes from oceanic subduction to continental collision through detrital zircon U-Pb and Lu-Hf isotope data: an example from the Chinese West Tianshan Orogen. *Gondwana Research* **105**,185–200.

Wang M, Zhang JJ, Pei XZ, Liu K, Zhang B and Chen YX (2018a) Significant Carboniferous magmatism and continental growth in the northern West Tianshan orogen, NW China: revealed by detrital zircon U-Pb and Lu-Hf analyses for turbidites from the North Tianshan Accretionary Complex. *Journal of Geodynamics* **118**, 11–31.

Wang M, Zhang JJ, Pei XZ, Zhang B, Chen YX, Xiao ZB and Zheng YR (2018c) Detrital zircon U-Pb-Hf isotopes study of the Lower Carboniferous Anjihai Formation from the northern margin of the Yili Block, NW China. *Geological Journal* **53**, 223–236.

Wang M, Zhang JJ, Qi GW and Liu J (2014) Geochemistry and geochronology of Early Permian acid volcanic rocks along Kuqa River and its tectonic implication in the southern margin of South Tianshan Orogen, Xinjiang. *Chinese Journal of Geology* **49**, 242–258.

Wang M, Zhang JJ, Zhang B, Liu K and Ge MH (2016a) Bi-directional subduction of the South Tianshan Ocean during the Late Silurian: magmatic records from both the southern Central Tianshan Block and northern Tarim Craton. *Journal of Asian Earth Sciences* **128**, 64–78.

Windley BF, AlexeIev D, Xiao WJ, Kröner A and Badarch G (2007) Tectonic models for accretion of the Central Asian Orogenic Belt. *Journal of the Geological Society, London* **164**, 31–47.

XBGMR (1993) *Regional Geology of Xinjiang Uygur Autonomy Region*. Beijing: Geological Publishing House.

Xia LQ, Xu XY, Xia ZC, Li XM, Ma ZP and Wang LS (2004) Petrogenesis of Carboniferous rift-related volcanic rocks in the Tianshan, northwestern China. *Geological Society of America Bulletin* **116**, 419–433.

Xiao WJ, Windley BF, Allen MB and Han CM (2013) Paleozoic multiple accretionary and collisional tectonics of the Chinese Tianshan orogenic collage. *Gondwana Research* **23**, 1316–1341.

Xiao XC, Tang YQ, Feng YM, Zhu BQ, Li JY and Zhao M (1992) *Tectonic Evolution of the Northern Xinjiang and its Adjacent Regions*. Beijing: Geological Publishing House, pp. 1–169.

Xie W, Luo ZY, Xu YG, Chen YB, Hong LB, Ma L and Ma Q (2016) Petrogenesis and geochemistry of the late Carboniferous reararc (or back-arc) pillow basaltic lava in the Bogda Mountains, Chinese north Tianshan. *Lithos* **244**, 30–42.

Xu XW, Li XH, Jiang N, Li Q, Qu X, Yang YH, Zhou G and Dong LH (2015) Basement nature and origin of the Junggar terrane: new zircon U–Pb–Hf isotope evidence from Paleozoic rocks and their enclaves. *Gondwana Research* **28**, 288–310

Xu XY, Li XM, Ma ZP, Xia LQ, Xia ZC and Peng SX (2006b) LA-ICPMS zircon U-Pb dating of gabbro from the Bayingou ophiolite in the Northern Tianshan Mountains. *Acta Geologica Sinica* **80**, 1168–1176.

Xu XY, Wang HL, Li P, Chen JL, Ma ZP, Zhu T, Wang N and Dong YP (2013) Geochemistry and geochronology of Paleozoic intrusions in the Nalati (Narati) area in western Tianshan, Xinjiang, China: implications for Paleozoic tectonic evolution. *Journal of Asian Earth Sciences* **72**, 33–62.

Xu XY, Xia LQ, Ma ZP, Wang YB, Xia ZC, Li XM and Wang LS (2006a) SHRIMP zircon U-Pb geochronology of the plagiogranite from Bayingou ophiolite in North Tianshan mountains and the petrogenesis of the ophiolite. *Acta Petrologica Sinica* **22**, 83–94.

Yang GX, Li YJ, Kerr AC and Tong LL (2018) Accreted seamounts in North Tianshan, NW China: implication for the evolution of the Central Asian Orogenic Belt. *Journal of Asian Earth Sciences* **153**, 223–237.

Zhang JJ, Wang T, Tong Y, Zhang Z, Song P, Zhang L, Huang H, Guo L and Hou Z (2017) Tracking deep ancient crustal components by xenocrystic/inherited zircons of Palaeozoic felsic igneous rocks from the Altai-East Junggar terrane and adjacent regions, western Central Asian Orogenic Belt and its tectonic significance. *International Geology Review* **59**, 2021–2040

Zhang KJ (2004) Secular geochemical variations of the Lower Cretaceous siliciclastic rocks from central Tibet (China) indicate a tectonic transition from continental collision to back-arc rifting. *Earth and Planetary Science Letters* **229**, 73–89.

Zhang W, Hu ZC and Liu YS (2020) Iso-Compass: new freeware software for isotopic data reduction of LA-MC-ICP-MS. *Journal of Analytical Atomic Spectrometry* **35**, 1087–1096.

Zheng H, Zhong LF, Wang R, Yang LH, Kapsiotis A, Xiao Y and Wan ZF (2019) Geochemistry and geochronology of mafic rocks from the Jinghe ophiolitic melange, northwest China: implications for plume-related magmatism and accretionary processes within the North Tianshan Ocean. *Lithos* **350**, 105246.

Zhong LL, Wang B, Alexeiev DV, Cao YC, Biske Y., Liu HS, Zhai YZ and Xing LZ (2017) Paleozoic multi-stage accretionary evolution of the SW Chinese Tianshan: new constraints from plutonic complex in the Nalati Range. *Gondwana Research* **45**, 254–274.